ingegneria sismica
International Journal of Earthquake Engineering
Anno XXXVIII – Num.2 - 2021

NONLINEAR STATIC AND INCREMENTAL DYNAMIC ANALYSES FOR SEISMIC DOWN-AISLE BEHAVIOR OF RACK STRUCTURES

Alessandro Mei, Maurizio Orlando, Luca Salvatori, Paolo Spinelli

Department of Civil and Environmental Engineering, University of Florence, Italy

SUMMARY: *A numerical campaign comparing the seismic behavior of cold-formed steel rack structures using both Nonlinear Static Analysis (NSA) and Incremental Dynamic Analyses (IDA) is presented. A total of 140 progressively scaled natural ground-motion records, along with 2 different forces distribution for NSA, were applied to a case study model build considering geometrical nonlinearity (P-Δ effects) and using proper elements to reproduce the pinching of beam-to-column joints in case of hogging and sagging bending moment. Data obtained from IDA were statistically processed and compared with the ones from NSA in terms of seismic vulnerability, specifically in terms of displacement demand and capacity, collapse spectral acceleration and proposing an appropriate damage index capable of tracking the state of the system as the spectral acceleration increase. Results show that NSA underestimates the displacement demand of the system and overestimates the collapse intensity measure (capacity spectral acceleration), thus not always being on the safe side.*

KEYWORDS: *Cold-Formed Steel, Nonlinear Static Analysis, Incremental Dynamic Analysis, Seismic Assessment, Damage Index*

1 Introduction

In an increasingly connected world, in which goods travel continuously on standardized pallets, the need for heavy storage facilities has led more and more companies, manufacturing and cooperatives to invest in bigger and taller rack structures made with cold-formed steel (CFS). To design carefully a rack means to protect what it carries, which is often more valuable than the rack itself.

The use of CFS led to very light structures made with thin-walled cross-sections, usually channels for vertical members (= uprights) and box for horizontal members (= beams) so that the amount of steel is considerably reduced if compared to hot-rolled counterparts, with obvious economical benefit. Other worthy advantages of rack structures are the great versatility in layouts, thanks to their special joints, and the fast assembly that further reduces the total cost of the rack. Rack structures also have some peculiar mechanical features that made them quite studied in the technical literature of the last few years. Maybe the easiest to note is the perforated, open sections of the uprights. As mentioned before, uprights are usually made with a channel section, bent to reduce local and distortional buckling phenomena [Baldassino *et al.*, 2019; Bertocci *et al.*, 2017; Foraboschi, 2019; Orlando *et al.*, 2017; Roure *et al.*, 2011; Zhao *et al.*, 2017] caused by the small thickness of the sections (typically from 1.5 mm to 3.0 mm). Uprights have also mono-symmetrical sections so that the centroid does not coincide with the shear center, resulting in shear-torsion coupling [Bernuzzi, Gobetti, *et al.*, 2014; Bernuzzi, Pieri, *et al.*, 2014; Gabbianelli et al., 2017; Rossi *et al.*, 2010], this peculiarity also led researchers to

Corresponding author: Alessandro Mei, Department of Civil and Environmental Engineering, University of Florence, Italy.
Email: alessandro.mei@unifi.it

consider 7-degree-of-freedom per node element for taking into account this phenomenon [Bernuzzi, Gobetti, *et al.*, 2014; Bernuzzi, Pieri, *et al.*, 2014].
The nonlinear behavior of the beam-to-column joints is also noteworthy. This kind of joint is usually made with a boltless connector, welded to the horizontal beam. The connector has a variable number of tabs that hook inside the spaced holes in the upright. Evaluating the mechanical behavior of a steel rack joint is difficult to do theoretically because of the great number of different upright-to-beam joints and different profiles used as uprights or beams. Nowadays, steel rack design codes (e.g. [CEN European Committee for Standardization, 2009]) require specific tests to evaluate moment-rotation constitutive laws of joints. Upright-to-beam joints in racks are also the main cause of energy dissipation during seismic motion, hence their importance in performance-based design. Uprights and beams are usually class-3 or -4 sections, according to Eurocode 3 [EN1993-1-1, 2005], so they behave elastically up to failure, without a stable hysteretic behavior. Monotonic and cyclic tests have been carried out in the last two decades over steel rack joints [Aguirre, 2005; Bernuzzi and Castiglioni, 2001; Dai *et al.*, 2018; Gusella *et al.*, 2018; Yin *et al.*, 2016], highlighting the pinching behavior of this kind of connections [Gusella *et al.*, 2019; Jovanović *et al.*, 2019; Peterman *et al.*, 2014; Zhao *et al.*, 2018]. Energy dissipation could occur in the base plates [Gilbert and Rasmussen, 2011; Petrone *et al.*, 2016] which show a nonlinear behavior that depends also on the axial load on the upright. Base plates can be studied together with seismic isolators [Filiatrault *et al.*, 2008; Kilar *et al.*, 2011; Simoncelli *et al.*, 2020] to reduce earthquake lateral forces on the main structure. Along with isolators, in recent years also non-standard design methods [Bernuzzi and Simoncelli, 2016; Montuori *et al.*, 2019] have been studied to overcome some lacks in standard codes.
The European provision for seismic design of racks is the EN 16681 [CEN European Committee for Standardization, 2016]. According to it, is possible to design a rack in seismic areas through two different methodologies: low-dissipative concept and dissipative concept. In the first case, the behavior factor must be lower than or equal to 2 (and depends on the adopted bracing configuration), while in the second one it can be greater than 2. In the dissipative case, the code considers four different types of analysis depending on the value of the factor θ, which is the inter-story drift sensitivity coefficient, defined as $\theta = \max[\theta_i]$ where

$$\theta_i = \frac{P_{E,i}\, d_{r,i}}{V_{R,i}\, h_i}, \tag{1}$$

being θ_i the inter-story drift sensitivity coefficient for the i-th story, $P_{E,i}$ the total gravity load on the considered story in seismic combination, $d_{r,i}$ the design inter-story drift evaluated as the difference of the average lateral displacement at the top and bottom of the story under consideration (for this purpose, the displacement is determined by using the lateral force method of analysis), $V_{R,i}$ the total seismic story shear, and h_i the inter-story height above the considered story. If $0.3 \leq \theta \leq 0.5$, the designer can choose between pushover-analysis with P-Δ geometrical effects or LDMA (Large Displacement Method of Analysis), as stated by Table 3 in EN 16681, for the seismic design of the rack; then if $\theta > 0.5$, the code forces to use a nonlinear time-history analysis with geometrical and constitutive nonlinearities. Also, it is worth noting that there is no upper bound for θ. In addition, rack structures are subjected to a limitation in terms of vertical loads; EN 16681 limits the critical load multiplier of a rack specifying that the ratio $P_E/P_{cr,E} \leq 0.5$, where P_E is the gravity load in seismic condition on the rack and $P_{cr,E}$ is the Euler critical load.

Since rack structures are very sensitive to second-order effects due to their high live-to-dead load ratios and their large deformability to horizontal loads, pushover analysis seems a reliable method to study and design racks in seismic areas [Bernuzzi *et al.*, 2017; Kanyilmaz, Brambilla, *et al.*, 2016; Kanyilmaz, Castiglioni, *et al.*, 2016]. Pushover analysis is accepted for rack structures using the method presented in the EC8 (EN1998-1-1, 2004), which is based on the N2 method [Fajfar, 2000]. Therefore, full-scale pushover experimental tests have been carried out for rack structures [Bernuzzi *et al.*, 2017; Comparini *et al.*, 2017; Kanyilmaz, Brambilla, *et al.*, 2016; Kanyilmaz, Castiglioni, *et al.*, 2016] to evaluate capacity curves and structural ductility factor. The results of the cited references focus primarily on the general behavior of the rack, the type of collapse, and evaluating the *q*-factor; some of the tested racks show a relatively ductile behavior and the *q*-factor commonly used in the design seems quite reliable.
However, in pushover analysis the hysteretic response of the upright-to-beam joints is neglected; this may lead to issues for rack structures that show unstable hysteretic behavior with pinching. Moreover, classical pushover analysis is based on time-independent modal shapes. So, it is in principle inaccurate for structures where higher mode effects are significant as rack structures. Finally, the equal-displacement rule for structures with large natural periods, on which the NSA analysis of the codes is based, may result in too small inelastic displacement demands in the case of hysteretic loops with significant pinching or stiffness or strength deterioration [Fajfar and Gašperšič, 1996; Rahnama and Krawinkler, 1993][Rahnama and Krawinkler, 1993][Rahnama and Krawinkler, 1993].
Here, the main goal is to investigate the effectiveness of the NSA for cold-formed steel rack structures in terms of displacement capacity and demand. The work is organized as follows: in Section 2, the considered case study is described, namely a rack previously subject of experimental tests; in Section 3, the numerical modeling via finite elements is presented; in Section 4, the nonlinear seismic analyses, considering both static pushover analysis and incremental dynamic analysis are shown; in Section 5, the results from the different analysis approach are described; finally, in Section 6, some concluding remarks are reported. This paper marks a starting point in that direction, making a comparison between NSA and IDA to better understand down-aisle rack seismic behavior and displacement demand for a sample rack structure as the seismic action increases.

2 Case Study

A two-bay, four-story pallet rack with a bay length of 2800 mm and an inter-story height of 2000 mm (Figure 1) is considered. This peculiar configuration was experimentally tested as a part of the research program StruMetaL (Italian acronym for “Lightweight steel structures for self-supporting warehouses with large storage capacity” [Comparini *et al.*, 2017]).
It is a common practice to have no bracing in the down-aisle direction, as bracings would render the handling of goods difficult in that direction. For this reason, the case study rack is braced only in the cross-aisle direction. Uprights are non-standard sections denoted as “130/250” and beams are “T1352” (Figure 2) with connector “type-D” joints [Gusella *et al.*, 2018]. The non-dimensional geometric properties of the cross-sections are reported in Table 1.
The steel used is S350GD for the uprights and S250GD for the beams with a yielding strength of 350 MPa and 250 MPa, respectively.
Applied vertical loads are given by two 800-kg pallets per bay at all levels, for a total mass of 12800 kg. The vertical load in place for the analyses corresponds to the maximum load, which

the structure would be designed for with the linear dynamic analysis and $S \cdot a_g = 0.27g$, where S is the soil factor and a_g is the peak acceleration at the bedrock.

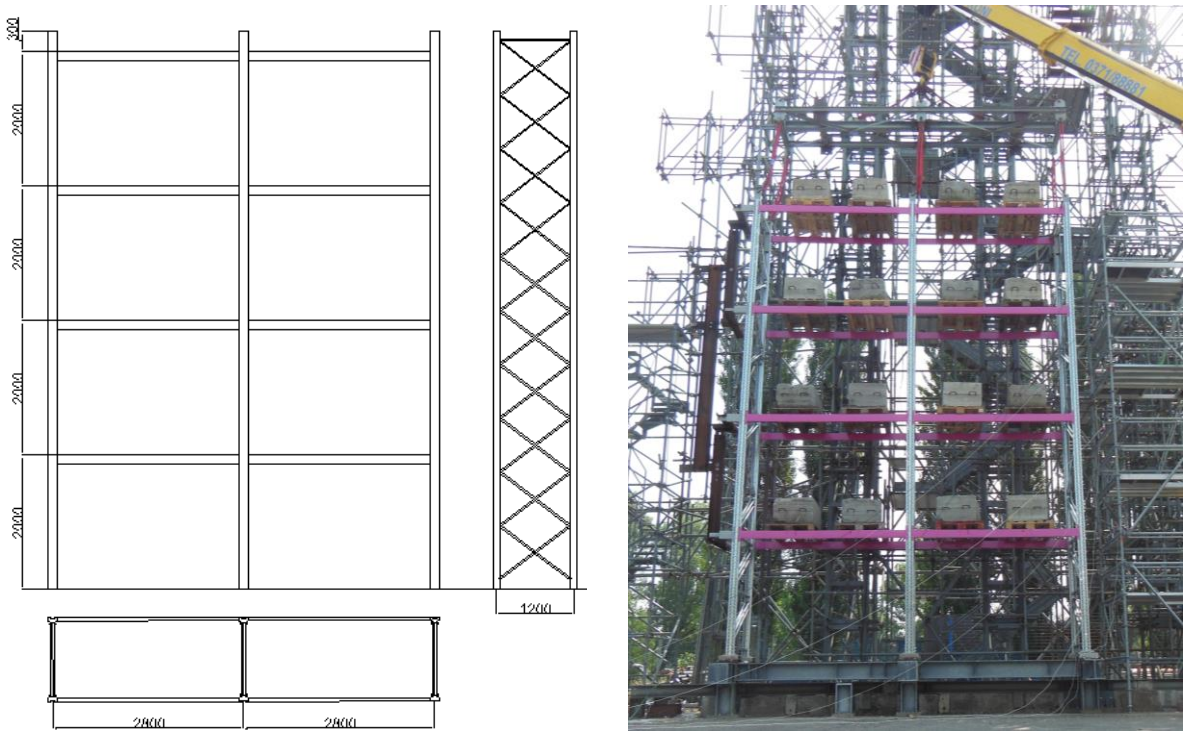

(a) *(b)*

Figure 1 - *(a) rack geometry (lengths in mm); (b) experimental test*

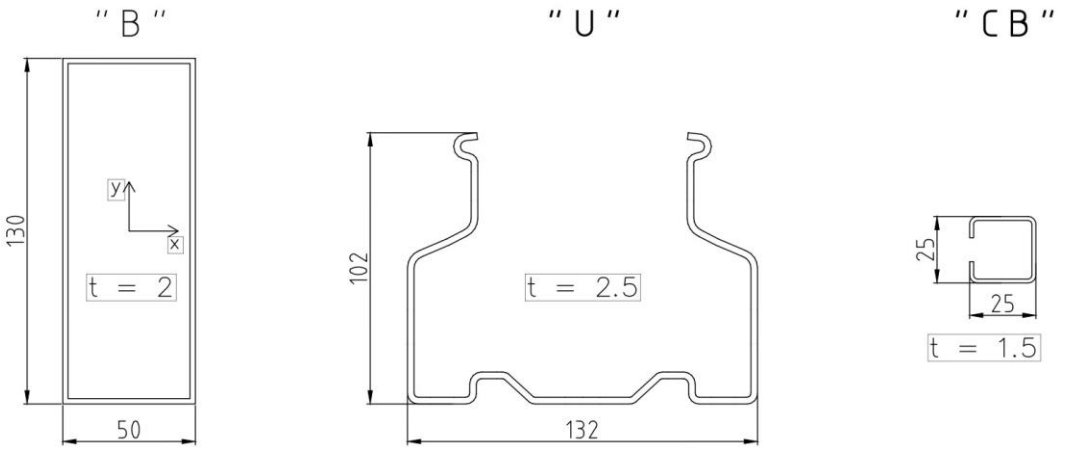

(a) *(b)* *(c)*

Figure 2 - *Cross-sections of beams (a), uprights (b), and cross-aisle bracing (c)*

Table 1 - *Geometric proprieties of cross-sections (ratios to section B)*

	B	U	CB
$A_g/A_{g(B)}$	1.00	1.38	0.17
$J_x/J_{x(B)}$	1.00	0.74	0.01
$J_y/J_{y(B)}$	1.00	7.04	0.03
$W_x/W_{x(B)}$	1.00	0.74	0.04
$W_y/W_{y(B)}$	1.00	2.69	0.06

3 Numerical Model

The rack mechanical model (Figure 3) was carried out using the finite element commercial software SAP2000 [SAP 2000, 2016].

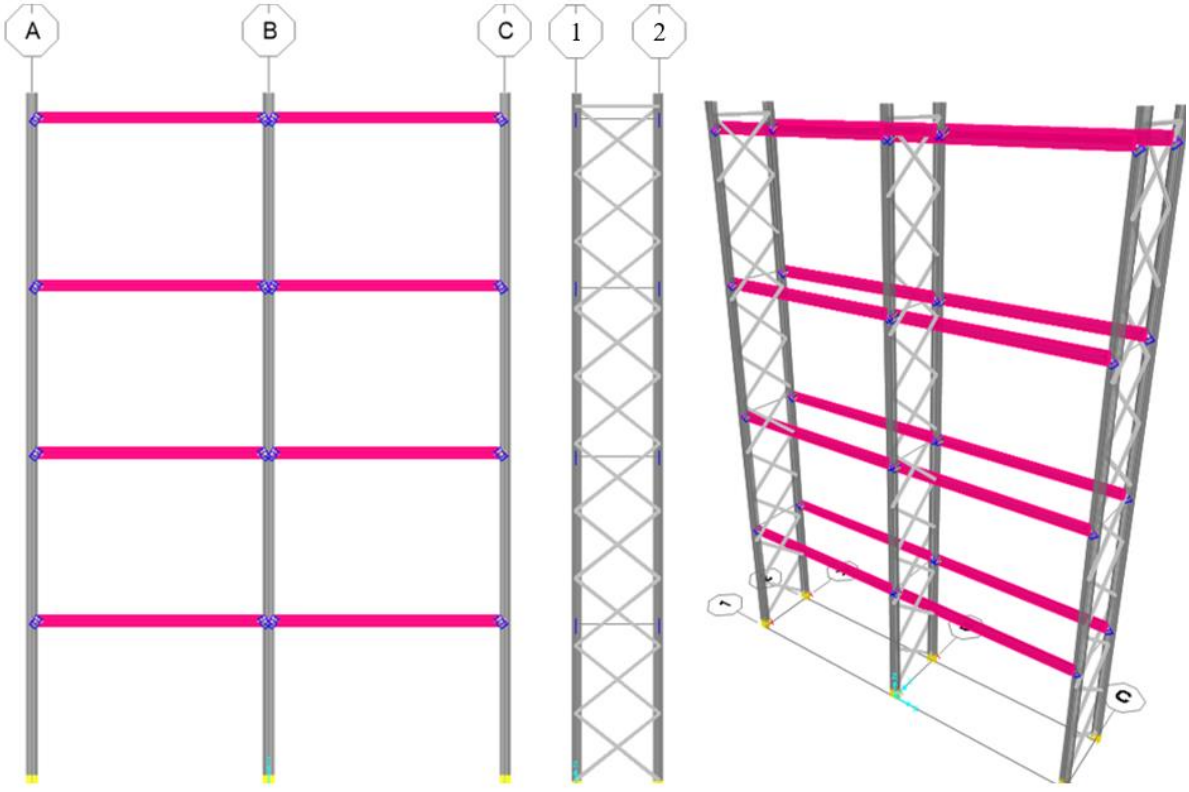

(a) *(b)* *(c)*

Figure 3 - *FE model views: down-aisle (a), cross-aisle (b) and isometric (c)*

The model is made using a six-degrees-of-freedom beam element. The upright area used for the elements is obtained via stub-column tests so that the influence of the holes on the behavior is taken into account, while moments of inertia refer to the gross section.
From the constitutive point of view, uprights and beams are modeled as linear elastic elements. Appropriate modeling of the pinching behavior of connections represented the most delicate

aspect. A scheme of the constitutive behavior is illustrated in Figure 4, where five branches can be distinguished:

- Branch 1: It is the linear-elastic branch; tabs deformation is reversible; the stiffness in this phase is that of modal and linear analysis cases;
- Branch 2: The rotation is such that the components of the connection undergo permanent deformations, starting with the tabs in the most eccentric position with respect to the centerline of the joint connection; the plastic phase is progressively entered and the stiffness of the union begins to decrease;
- Branch 3: During the unloading, the connection elements regain the elastic part of their deformation; however, due to the excursion into the plastic regime, deformations will not return to the situation prior to application of the load;
- Branch 4: Pinching. The tabs have undergone plastic deformation to such an extent that the perfect fitting to the holes in the uprights is no longer allowed. When the load is reversed, the union undergoes a rapid rotation, which stops only when the tabs start reacting in the opposite direction;
- Branch 5: Tabs act again elastically but in the direction opposite to the one of Branch 1.

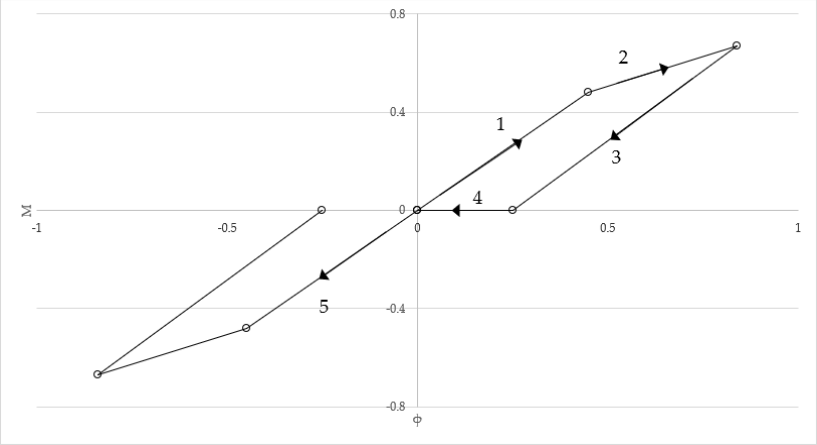

Figure 4 - *Scheme of the pinching moment (vertical axis) - rotation (horizontal axis) behavior*

As the amplitude of rotation cycles increases, the extent of Branch 4 will increase: the plastic deformations of the joint tabs are such that when the load is reversed there will be a moment-free rotation. The larger the amplitude of cycles the greater the rotation of the tabs, compared to its original configuration. The tab will tend to open up, which creates an even greater rotational gap between upright and beam. Therefore, a mechanical model that takes into account the phenomenon of pinching is necessary. The hysteretic cycles dissipate less energy than the typical elastic-plastic ones characterizing hot-rolled steel or reinforced concrete.
The adopted joint model is a slight modification of the one proposed by [Comparini *et al.*, 2017] (see also [Gusella *et al.*, 2019]). It is based on a combination of gap/hook, multilinear plastic, and rigid elements (Figure 5). The nonlinearities are due to four links acting on the rotation (R3), a gap in series with a multilinear plastic element, both in parallel with a hook in series with a multilinear plastic element. The gap and the hook are nonlinear elastic elements that allow one of the plastic elements to work for positive rotations and the other one for negative rotations, reacting respectively only to compressive and tensile stress.

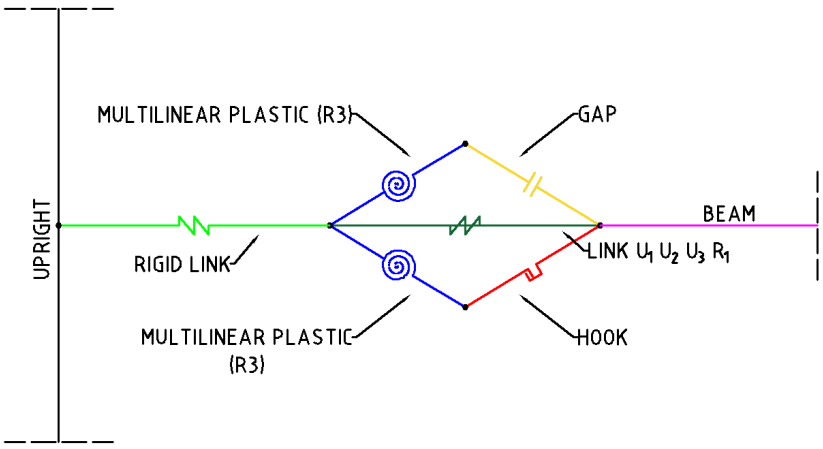

Figure 5 - *Proposed joint model*

The plastic elements model the nonlinear monotonic loading curve and the permanent plastic deformation of the tabs by a single internal variable (plastic rotation) each. The parallel allows two different plastic deformation to be reproduced for positive and negative rotations, as well as the pinching effect.

The input moment-rotation curve for the multilinear links was taken as coincident with the envelope of the experimental cyclic tests for type-D joints made by [Gusella *et al.*, 2018]. To assess the validity of the joint model, the experimental campaign has been simulated and compared with the experimental data (Figure 6).

For the base joints of the uprights, a linear elastic rotational link was used [Comparini *et al.*, 2017]; the stiffness of the link has been calibrated using the capacity curve of a real scale test in the same loading condition, thus considering also the effect of vertical load on the performance of the base-plate connection. This choice is motivated by the absence of experimental data on the behavior of the base-plate connection; therefore, its dissipative behavior has been neglected. The factor θ of Equation (1) is equal to 0.3, which makes, according to code provisions, the structure susceptible to the second-order effects but not explicitly requiring time-history analyses.

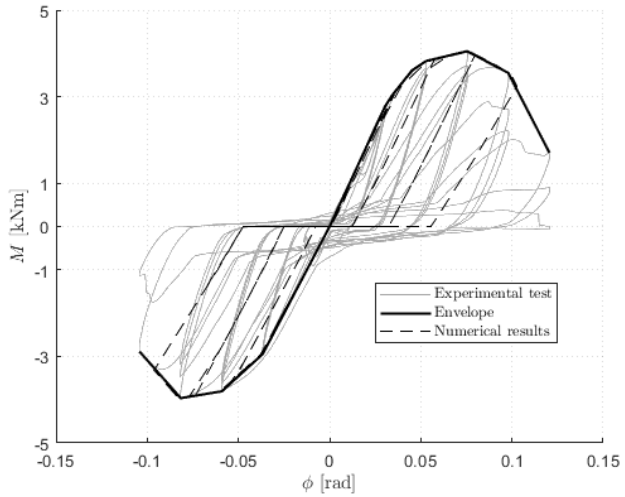

Figure 6 - *Comparison between experimental and numerical moment-rotation cyclic behavior*

The first period of the structure in the down-aisle direction is 2.48 s, while in the cross-aisle direction is 0.51s.
Besides the beam-to-upright nonlinear joints, full geometrical nonlinearities were accounted for both in the static and dynamic analyses.

4 Seismic Analyses

4.1 Seismic Input

Two seismic inputs were used: a pseudo-acceleration spectrum for NSA and a set of natural ground-motion records for IDA.
The pseudo-acceleration spectrum was defined considering medium-high seismicity with a class C soil according to EC8 [EN1998-1-1,2004]. Spectral parameters are reported in Table 2.

Table 2 - *Pseudo-acceleration spectrum parameters (the meaning of the symbol is the one of EC8 (EN1998-1-1, 2004), Italian national annex)*

T_r [years]	a_g [g]	F_o [-]	T_C^* [s]	T_B [s]	T_C [s]	T_D [s]	S [-]
475	0.1998	2.38	0.29	0.153	0.458	2.399	1.38

As to IDA, a set of seven ground acceleration time-histories of natural earthquakes were considered. The mean spectrum obtained from the records was required to be compatible with the target spectrum adopted for NSA. The record selection was carried out by using REXEL software [Iervolino *et al.*, 2010], with 10 % lower and 30 % upper tolerance for the average spectral matching for a natural period ranging from 0.15 s to 2.5 s. It was also required that the class of soil on which the seismic event was recorded is compatible with the class assumed in the analysis. Selected records are listed in Table 3, where sites and dates of the earthquakes are reported, together with the magnitude moment (M_w), the distance from the source to the recording site (R), the Peak Ground Acceleration (PGA) of the events (defined as the largest ground acceleration recorded during an earthquake) and the soil class of the site according to Eurocode 8. The response spectra for the records, their mean, and the comparison with the target spectrum are reported in Figure 7.

Table 3 - *List of seismic events selected*

ID	Event	Date	M_w	R [km]	PGA [m/s ^{2}]	Soil class (EC8)
#1	Darfield	3 Sep 2010	7.1	13.31	2.329	C
#2	Christchurch	21 Feb 2011	6.2	13.73	2.855	C
#3	Northridge	17 Jan 1994	6.7	20.19	2.507	C
#4	Miyagi Pref.	25 Jul 2003	6.1	9.93	1.951	C
#5	Suruga Bay	10 Aug 2009	6.2	18.45	2.883	C
#6	Northridge	17 Jan 1994	6.7	11.02	3.374	C
#7	Loma Prieta	18 Oct 1989	6.9	29.66	3.161	C
Mean	-	-	6.6	16.6	2.723	-

Note: PGAs refer to the unscaled event.

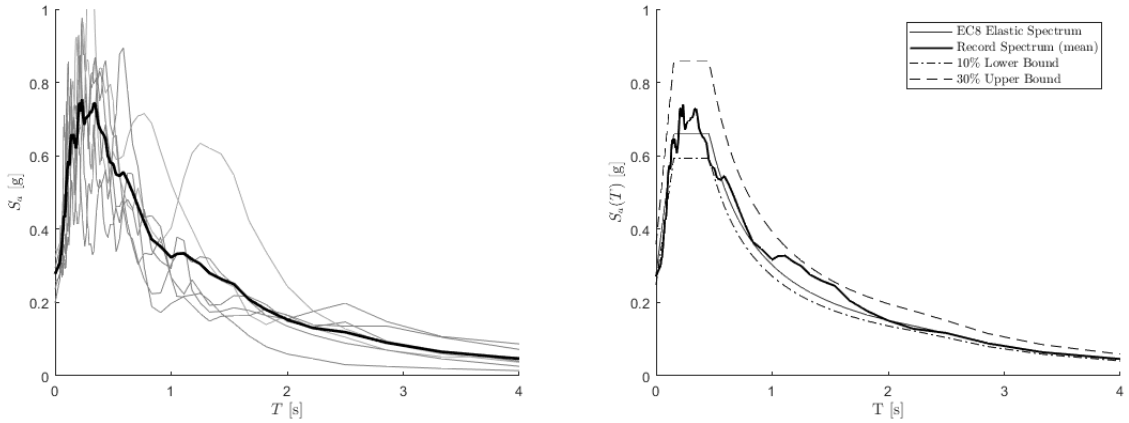

v(a) *(b)*

Figure 7 - *Pseudo-acceleration response spectra: (a) selected earthquakes and their mean (thick line), (b) comparison between record mean and target EC8 spectrum*

4.2 Identification of structure collapse and joint damage

As the uprights are class 3 or 4 sections, it is reasonable to expect a linear elastic behavior with no ductility. It is assumed that the entire structure fails at the collapse of the first upright and the analyses are stopped as soon as the failure condition is achieved so that no post-failure behavior is considered. Uprights are checked according to EN 15512 [CEN European Committee for Standardization, 2009] for bi-axial bending and compression with lateral-torsional buckling, namely by

$$\frac{N_{Ed}}{\chi_{min}\, A_{eff}\, f_y/\gamma_M} + \frac{k_{LT}\, M_{y,Ed}}{\chi_{LT}\, W_{y,eff}\, f_y/\gamma_M} + \frac{k_z\, M_{z,Ed}}{W_{z,eff}\, f_y/\gamma_M} \leq 1, \qquad (2)$$

where *y* is the major axes and the meaning of symbols is the same as in the referenced building code. The effective area was obtained via stub-column tests, while the effective section moduli via the effective area method according to Eurocode 3 [EN1993-1-3, 2005]. The inequality in Equation (2) is checked for every load step (for NSAs) or time step (for IDAs) and every upright of the rack. This approach makes it possible to identify whether, when, and where a violation of Equation (2) occurs. The first step for which the inequality in Equation (2) is violated for any of the uprights is assumed as the onset of global failure and the analysis is stopped.

The failure domain obtained using Equation (2) is reproduced in Figure 8a. It is worth noting that other experimental and numerical forms of the failure domain are available [Baldassino *et al.*, 2019; El-Kadi and Kiymaz, 2015; Elias *et al.*, 2018; Foraboschi, 2020], also for this specific upright [Bertocci *et al.*, 2017]; specifically, the latter domain is certainly optimized and more accurate but it was chosen to stay with regulatory failure domain due to different slenderness of the tested specimens versus the one used in the present analyses.

Beam-to-upright joint damage has been checked step-by-step with the procedure explained and according to the index introduced by [Powell and Allahabadi, 1988]:

$$I_{d_J} = \frac{\phi_i^j - \phi_E}{\phi_C - \phi_E} \tag{3}$$

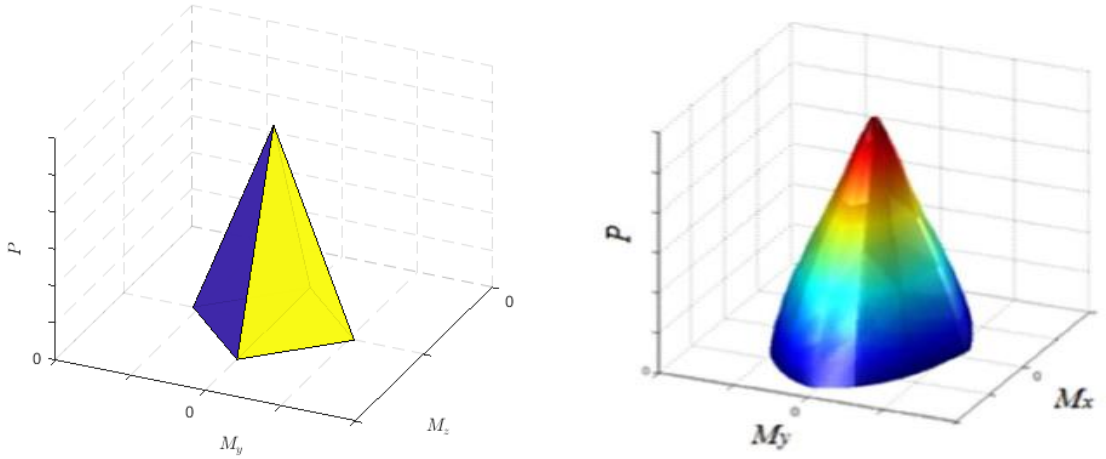

(a) *(b)*

Figure 8 - *Failure domains of uprights: (a) regulatory and (b) numerical* [Bertocci *et al.*, 2017]

Where ϕ_i^j is the rotation of the *i*-th node at the *j*-th step, ϕ_E is the linear elasticity limit, and ϕ_C is the rotation of the joint at 20% degradation of the peak moment in the cyclic envelope.

4.3 Nonlinear Static Analysis

NSAs were conducted by using the N2 method [Fajfar, 2000; Fajfar and Gašperšič, 1996] with the prescription of EC3 (EN1993-1-1, 2005). Two distributions of lateral loads were used: a triangular distribution and a uniform distribution. Forces from those patterns were applied at each story. Firstly, a nonlinear static analysis in load control is used to apply the gravity loads. Then, nonlinear static analyses in indirect control of the top-story displacement δ were performed. The top-story displacement at failure is the displacement capacity δ_u of the rack. The displacement demand δ_d was calculated using the mean response spectrum of the seven records.

Figure 9 presents the two capacity curves. The triangular distribution results in a higher base shear force at collapse but a smaller displacement capacity than the uniform distribution. The ultimate displacement is 0.64 m for the triangular distribution and 0.83 m for the uniform one. According to the N2 method, the displacement capacity is obtained by considering an equivalent SDOF system using a modal participation factor $\Gamma = \phi_1^t\, M\, \tau / (\phi_1^t\, M\, \phi_1) = 1.28$, where ϕ_1 represents the first modal shape vector normalized to unit displacement, M is the mass matrix and τ is the influence vector. The SDOF period was obtained as $T^* = 2\pi\sqrt{m^*/K^*}$ where m^* is the modal mass and K^* is the slope of the elastic section of the piecewise-linear equivalent capacity curve. A period $T_t^* = 2.34$ s was estimated for the triangular distribution and $T_u^* = 2.55$ s for the uniform distribution.

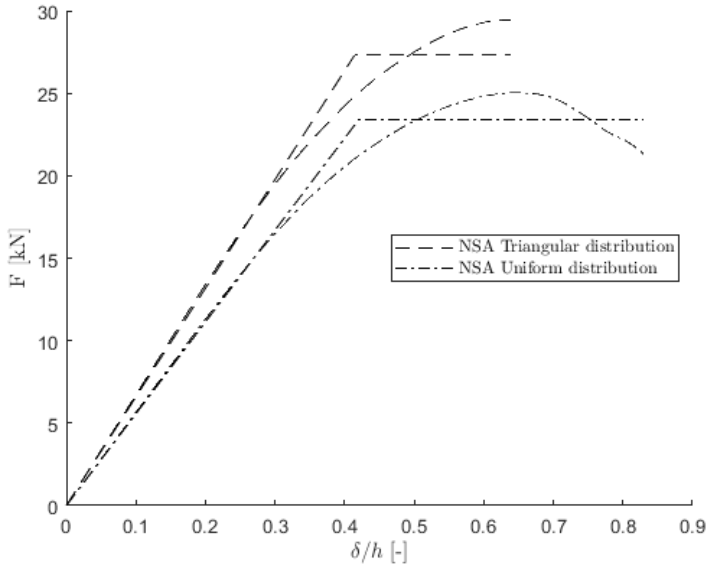

Figure 9 - *NSA capacity curves with corresponding piecewise linearizations*

Using the mean elastic spectrum, is it possible to evaluate the displacement demand for the SDOF system as $\delta_d^* = S_{de}(T^*)$ (because for this case study, as for virtually any rack, $T^* > T_C$), where S_{de} is the elastic displacement response spectrum. The rack displacement demand is then $\delta_d = \Gamma \delta_d^*$.
Deformed configurations at failure are reported in Figure 10.

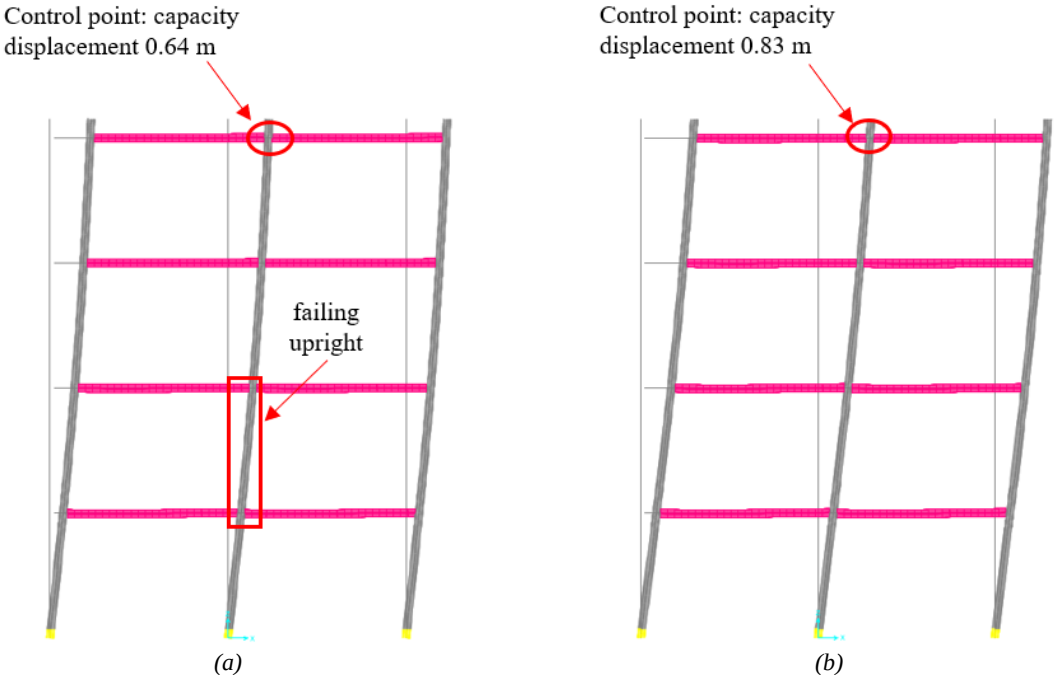

(a) *(b)*

Figure 10 - *Deformed configuration at ultimate displacement: triangular (a) and uniform (b) load distributions (deformed shapes have the same amplification factor)*

For the triangular load distribution, collapse occurs in second story central uprights and it is caused primarily by the bending moment acting in the plane of the rack, rather than by the axial load. This result is consistent with the relatively small height and loading of the case study. Interestingly, the rack subjected to the uniform force scheme does not collapse during the analysis that is interrupted when the conventional condition of shear-force decrease of 15% is reached.The damage level of the joints for the last step of the NSA analysis is reported in Figure 11.

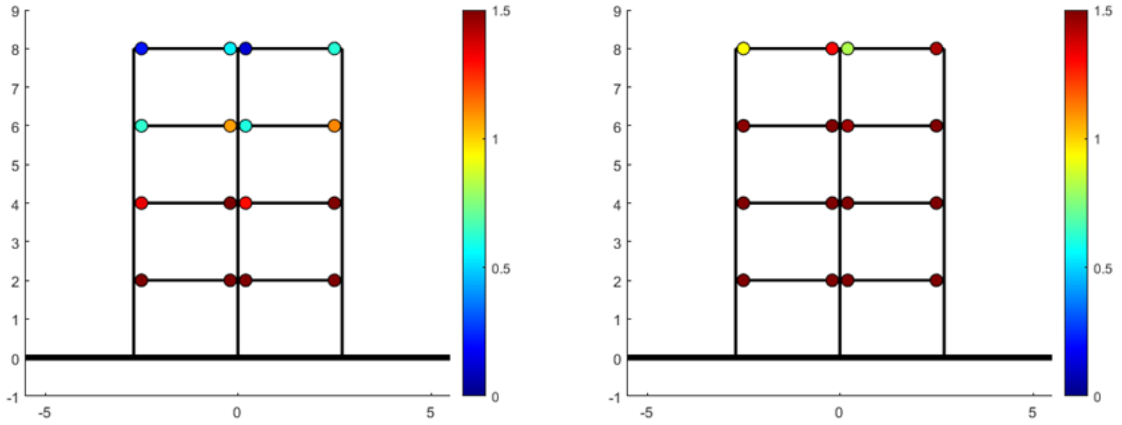

(a) *(b)*

Figure 11 - *Values of I_{d_J} at failure: triangular (a) and uniform (b) load patterns*

For both load distributions, several joints overcome their conventional rotation limit, thus I_d is greater than unity. However, the rack subjected to a triangular load distribution fails for smaller horizontal displacements and the values of the damage index are still smaller than unity in the top two stories. Conversely, the damage level of all joints in the model with the uniform load pattern has an index I_{d_J} greater than unity.

4.4 Incremental Dynamic Analysis

In an IDA, after the nonlinear static application of the vertical loads, a sequence of nonlinear dynamic analyses is performed by scaling the ground-motion records to which the structure is subjected by an increasing factor until collapse is reached during the simulation [Vamvatsikos and Cornell, 2002]. An IDA is, therefore, an evolutionary analysis that allows the exact understanding of the nonlinear phenomena that trigger and evolve during seismic events. As it is *incremental*, it allows a complete analysis of structural behavior evolution at the growing of the seismic intensity, permits to evaluate how the structure reaches the crisis, which type of crisis occurs and where are the structural weaknesses. Figure 12 reports the time-histories of displacement, relative velocity and relative acceleration of the top story, center node obtained by progressive scaling of record #1, highlighting how the structural response changes when the seismic action increases and nonlinear phenomena are triggered.
IDA results are presented using an *IDA plot*, which is composed of one curve for each seismic record (each curve is called a *single-record IDA curve*). An IDA curve represents the variation of an Engineering Demand Parameter (EDP) versus a seismic Intensity Measure (IM).

A single-record IDA curve requires scaling a certain seismic record by a factor incremented in steps; the stepwise procedure ends when the scaled record leads the structure to collapse.
IDAs are performed using a direct-integration scheme. The equations of motion are solved for every time-step (chosen as 0.05 s) using the Hilber-Hughes-Taylor algorithm [Hilber *et al.*, 1977] with parameters set to reduce it to the unconditionally stable average constant acceleration method. Rayleigh damping is used by setting the damping ratio equal to 5% around the natural period.

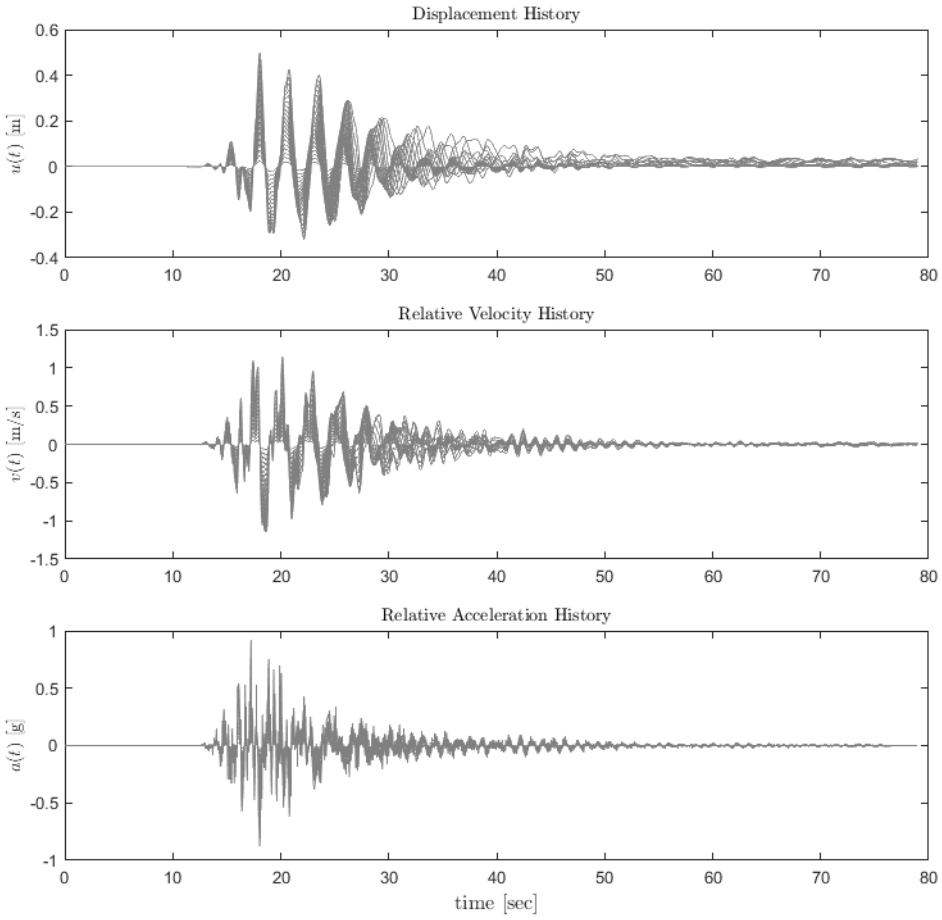

Figure 12 - *From top to bottom: displacement, relative velocity and relative acceleration time-histories obtained by the progressive scaling record #1*

For each scalar factor, the EDP is chosen as the maximum top horizontal displacement normalized to the rack height δ/H and the IM as the spectral ordinate of the pseudo-acceleration elastic response spectrum $S_a(T_1)$ of each scaled record at the first natural period T_1 of the rack. The plot in Figure 13 shows the IDA curves of the seven records progressively scaled up to collapse (represented by black dots).
Figure 14 shows the curves of the 16%, 50% and 84% percentiles, together with the mean values of the spectral acceleration of the single-record curves evaluated at constant drift δ/H. The collapse-point percentiles and mean, evaluated for both coordinates in the IDA plane, are also reported. It is worth noting that, because of the procedure described [Vamvatsikos and Cornell, 2004], the percentile and mean collapse points do not lie on the corresponding cross-sectional percentile or mean curve.

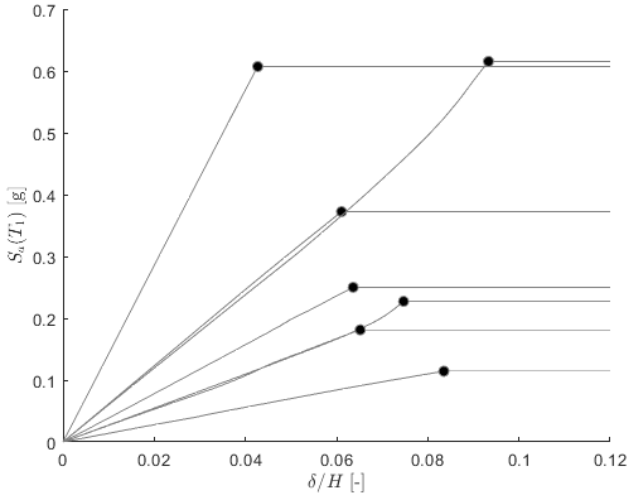

Figure 13 - *IDA plot with collapse points (black dots) for* EDP = δ/H

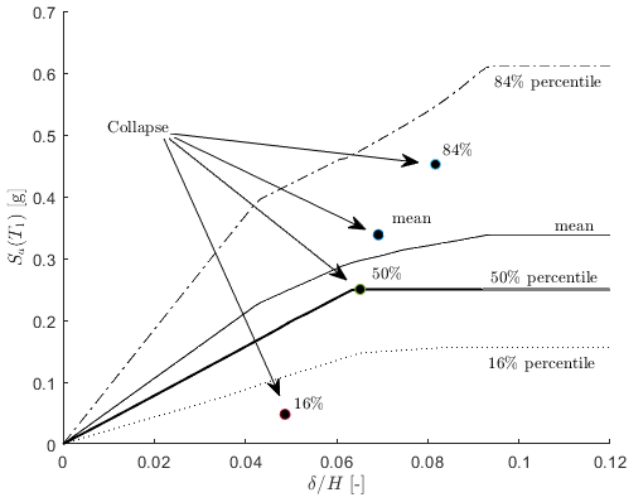

Figure 14 - *Constant-drift 16%-, 50%-, and 84%-percentile and mean IDA curve and collapse points for* EPD = δ/H

If it is assumed that the median could be used to estimate the safety of the structure, it can be seen that the sample rack can withstand an $S_a(T_1)$ of about $0.25g$, while, if the mean value is considered, the capacity IM is larger than $0.30\ g$.
A second IDA plot can be obtained by using EDP = $\Delta\delta/h$, i.e. the inter-story drift, obtained as the maximum inter-story displacement $\Delta\delta$ divided by the inter-story height h (Figure 15). Again, black dots serve as collapse identification points for every curve.
Statistical analyses of the IDA plot related to inter-story drift are reported in Figure 16.
The collapse mode for each record has also been investigated. Also with dynamic analysis, the collapse occurs mainly due to the bending moment; however, the failing uprights vary depending on the record considered (Table 4).

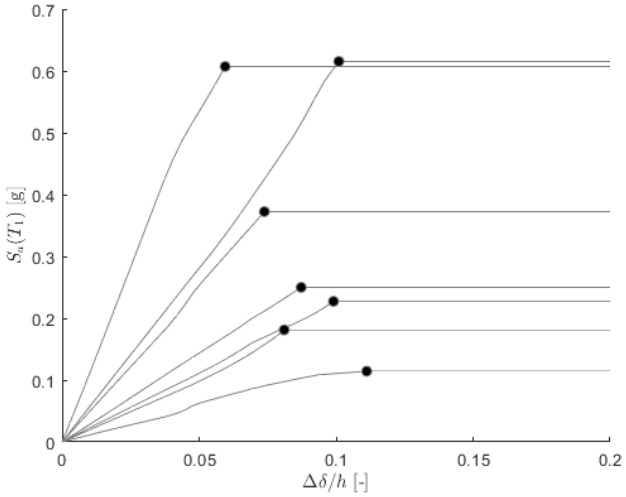

Figure 15 - *IDA plot with collapse points (black dots) for* EDP = $\Delta\delta/h$

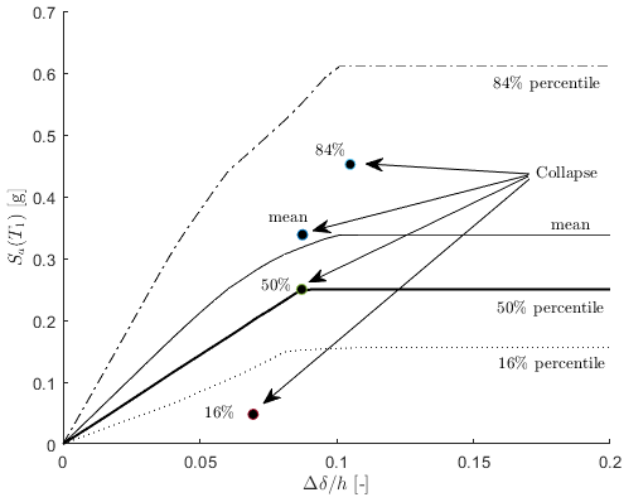

Figure 16 - *Constant-drift 16%-, 50%-, and 84%-percentile and mean IDA curve and collapse points for* EPD = $\Delta\delta/h$

Table 4 - *Identification of collapse for IDA analyses*

Record	#1	#2	#3	#4	#5	#6	#7
Collapse	2nd story, center	3rd story, center	2nd story, center	2nd story, center	3rd story, center	2nd story, center	2nd story, center

Generally, the failing upright is the same as the NSA; however, in record #2 and #5, collapse occurs at the third story. This difference can be explained by observing the deformed configurations at incipient collapse, reported in Figure 17, where the uprights undergo major deformation.

By projecting the deformation at failure over the modal base it is possible to estimate the contribution of each mode to failure. The results of such analysis are reported in Figure 18.

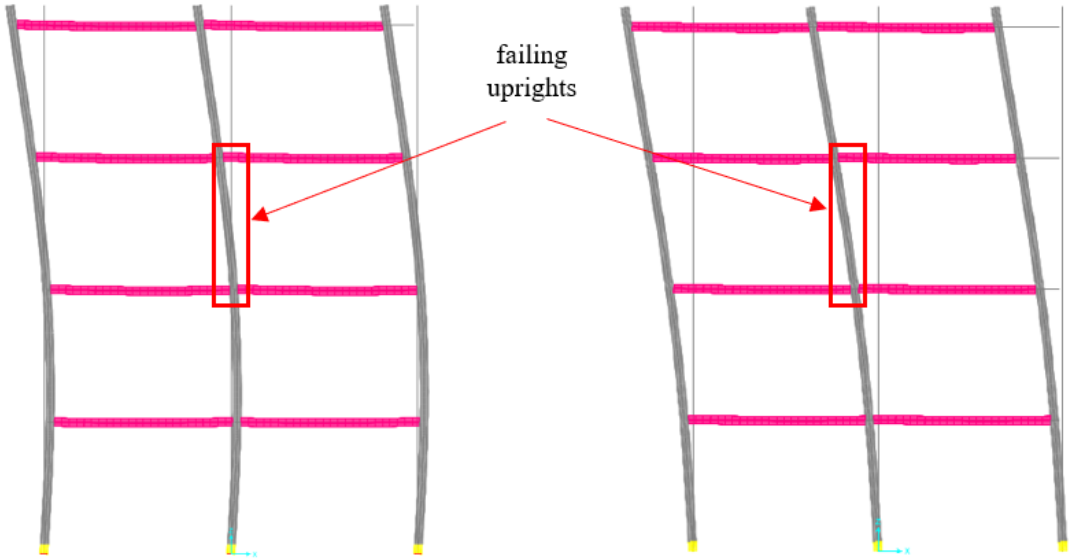

(a) *(b)*

Figure 17 - *Deformations at incipient collapse for records #2 (a) and #5 (b)*

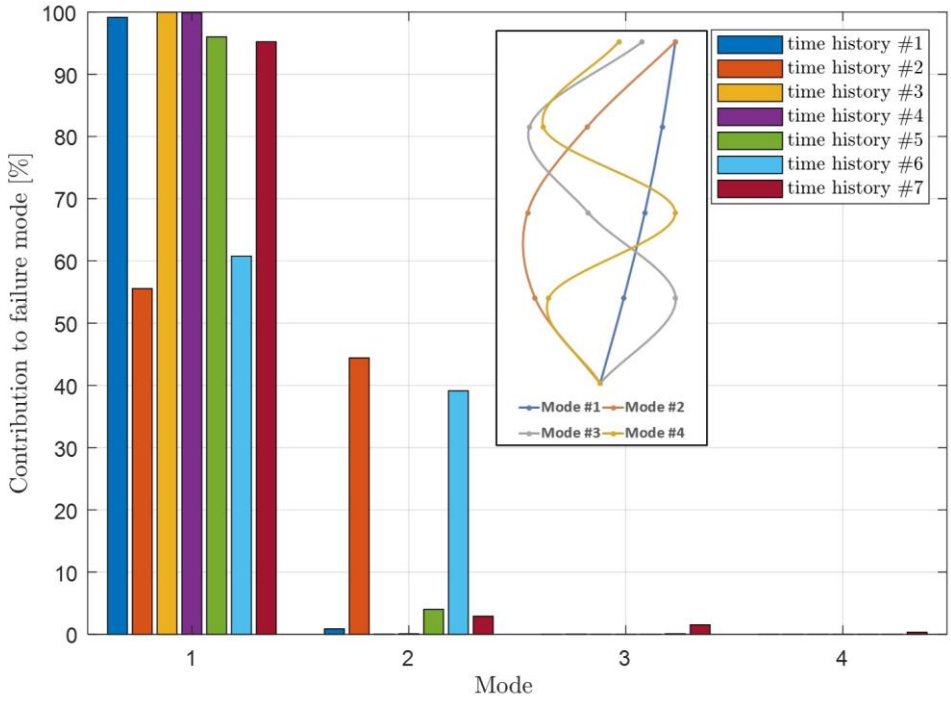

Figure 18 – *Contribution of each mode to failure*

For time-histories #2 and #6, a significant contribution of the second mode is highlighted.
In terms of beam-to-upright joint damage, data are reported using the maximum index values I_{d_J} of each record evaluated at the failure scaling factor. As an example, the damage evolution of record #3 is reported in Figure 19.
The mean joint damage at collapse is shown in Figure 20.

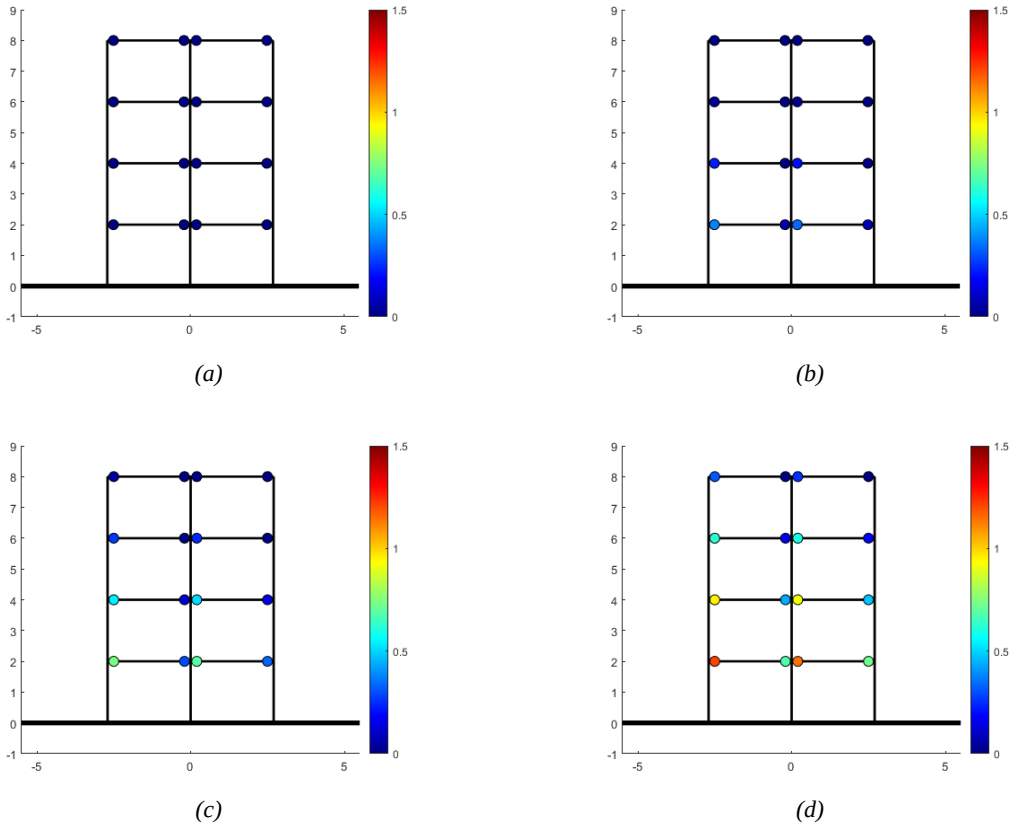

(a) *(b)*

(c) *(d)*

Figure 19 - *Joint damage evolution for record #3: $S_a(T_1)$ = 0.012 g (a), $S_a(T_1)$ = 0.137 g (b), $S_a(T_1)$ = 0.159 g (c), $S_a(T_1)$ = 0.215 g (d)*

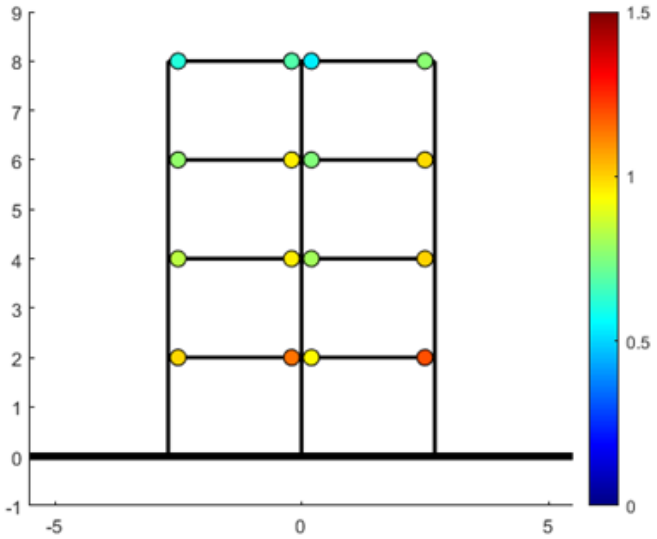

Figure 20 - *Mean joint damage at the collapse*

5 Comparison between IDA and NSA

The comparison between NSA and IDA in terms of base shear versus displacement is not meaningful, because of the presence of the inertia in the latter kind of analysis, while a more suitable comparison can be made in terms of seismic intensity measure versus displacement [Marra *et al.*, 2017].
Total and inter-story IDA curves (median and mean) are plotted and compared to the corresponding NSA curves with highlighted collapse points in Figure 21 and Figure 22, respectively. Collapse IMs are greater for NSA analyses, independently of the load distribution, than IDA median and IDA mean as visualized in Figure 23a.
To detail the comparison, the capacity and demand displacements are studied.
The comparison of displacement capacity is visualized in Figure 23b. Both median and mean IDA values smaller than NSA with equal-displacement rule between nonlinear and linear oscillators.

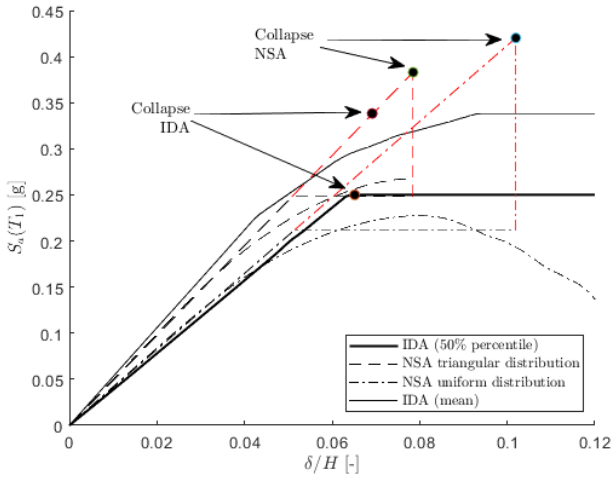

Figure 21 - *NSA vs IDA for* EDP = *δ/H*

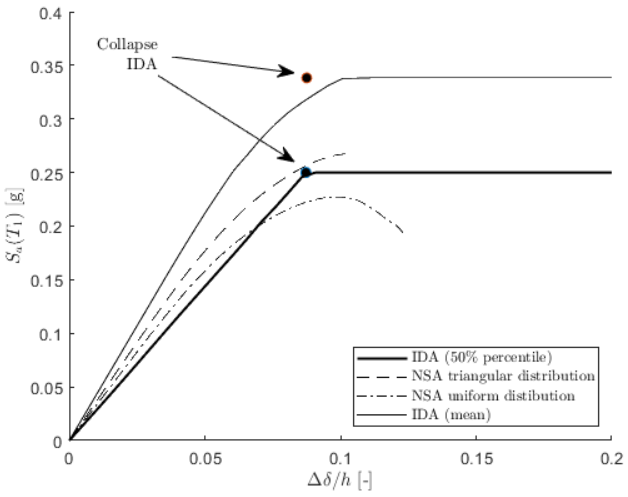

Figure 22 - *NSA vs. IDA for* EDP = *Δδ/h (collapse for NSA corresponds to the endpoint of each curve)*

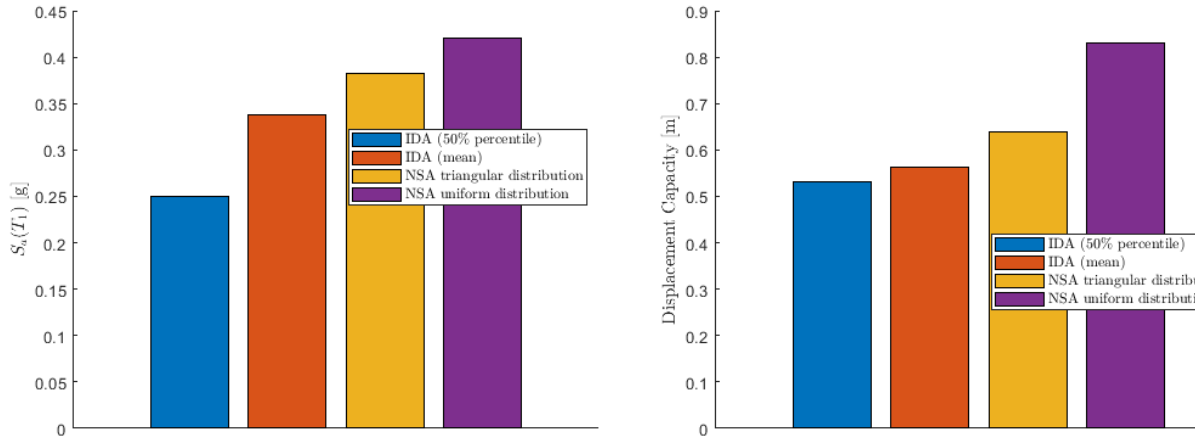

(a) *(b)*

Figure 23 - *Capacity IM (a) and displacement capacity (b)*

The comparison of displacement demands is reported in Figure 24. The displacement demand in the IDA is defined, for each value of the scaling factor, as the maximum displacement of the top of the structure during the time-history. The IDA displacement demand was plotted both in terms of mean and median. Displacement demand obtained from the median IDA is slightly larger than NSA for triangular load distribution, which is the largest of the two NSA displacement demands. Conversely, the mean IDA displacement demand is smaller than NSA for smaller values of the IM, but shows a remarkable and progressive increase of slope for IM values larger than 0.23 g, becoming larger than both NSA. Another comparison was made in terms of the ratio between displacement demand and ultimate displacement. This approach followed a methodology similar to the one exposed in [Powell and Allahabadi, 1988], where a damage index I_d was defined. Due to the difficulty to define a limit elastic displacement δ_e for this kind of structures, as the onset of plasticity in the beam-to-upright joints starts for quite small rotations, the index was rethought as:

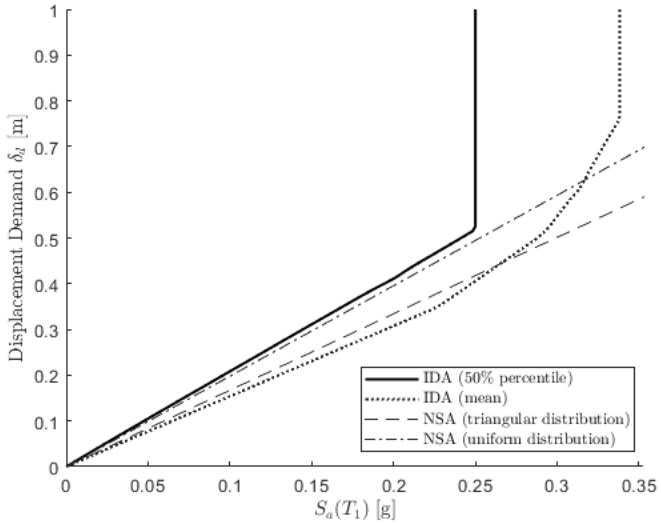

Figure 24 - *Displacement demand comparison*

$$I_d = \min\left(\frac{\delta_d}{\delta_u}; 1\right), \tag{4}$$

where δ_d is the displacement demand, defined above, and δ_u is defined for the IDA as the maximum displacement of the time-history with the largest scale factor for which the structure still does not collapse. As it was defined, I_d could be seen as a measure of the global damage of the rack. Values greater or equal than unity mean a collapsed structure (for which $\delta_d \geq \delta_u$). The results in terms of I_d against $S_a(T_1)$ are shown in Figure 25, where, for IDA, statistics of I_d are performed at constant $S_a(T_1)$. The median IDA damage index is always larger than NSA with both load distributions, i.e. the latter is not on the safe side. If the mean IDA damage index is considered this is still true for the smaller values of the IM.
The last comparison was made in terms of damage level of the joints. The definition of a damage level I_{d_J} allows understanding if joints go beyond their elastic phase and which joints undergo plastic deformations. Comparing Figure 11 and Figure 20, it is possible to note how the damage is more uniform in NSAs than in IDAs. In this latter analysis, only first story joints are damaged considerably and enter the plastic phase.

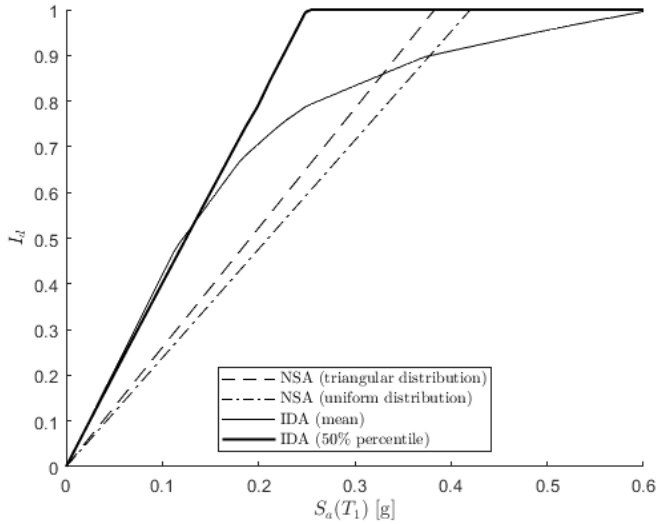

Figure 25 - *Global damage index vs. IM*

6 Concluding remarks

The goal of this study was to investigate the effectiveness of the N2 method for the down-aisle seismic analysis of a simple rack structure, as compared to the state-of-the-art analysis represented by IDA.
The main results can be summarized as follows:

- Displacement capacity obtained from NSA are larger than the corresponding ones obtained from IDA, both median and mean values; this can be explained by higher mode contributions to inter-story drift than in NSA;
- Capacity IM ($S_a(T_1)$) obtained from NSA are larger than the one obtained from both median and mean IDA;

- Displacement demand from NSA is smaller than or equal to the median IDA. The mean IDA displacement demand shows a remarkable nonlinearity, which highlights a possible limitation of the equal-displacement model. Hence, this model that holds for stable hysteresis cycles may be unsuitable for rack structures characterized by the pinching behavior of beam-to-uprights joints and remarkable P-Δ effects;
- The damage index obtained from NSA is always smaller than the corresponding median IDA; also in the case of mean IDA, the damage index is larger for the weaker earthquakes.

Results refer to a specific case study but highlighted how pushover analysis is not always on the safe side. The present analyses need to be expanded in terms of geometries, beam-to-column constitutive laws and different live loads. If the results from the parametric expanded study will confirm this behavior, it will be possible to start thinking about adjusting the N2 method specifically for CFS racks.

7 Acknowledgements

The authors are thankful to Claudio Pagani, Stefano Lombardi, and Federico Gusella for their supporting work.

Appendix - Calibration of the FE model

In this appendix, the results obtained from the calibration of the model are presented.
The moment-rotation curve for the beam-to-upright joints was the one obtained by monotonic experimental tests [Gusella *et al.*, 2018]. Conversely, the experimental moment-rotation curve for the base joints was not available. For this connection, a linear elastic moment-rotation constant was calibrated by comparing the global pushover curve of the rack obtained experimentally [Comparini *et al.*, 2017], with the numerical one (Figure 26). That study also investigated numerically the potential failure mechanism, which was not reached during the experimental test: the rack fails due to buckling of an upright and no sufficient rotations are reached to induce the failure of the beam-to-column joints.

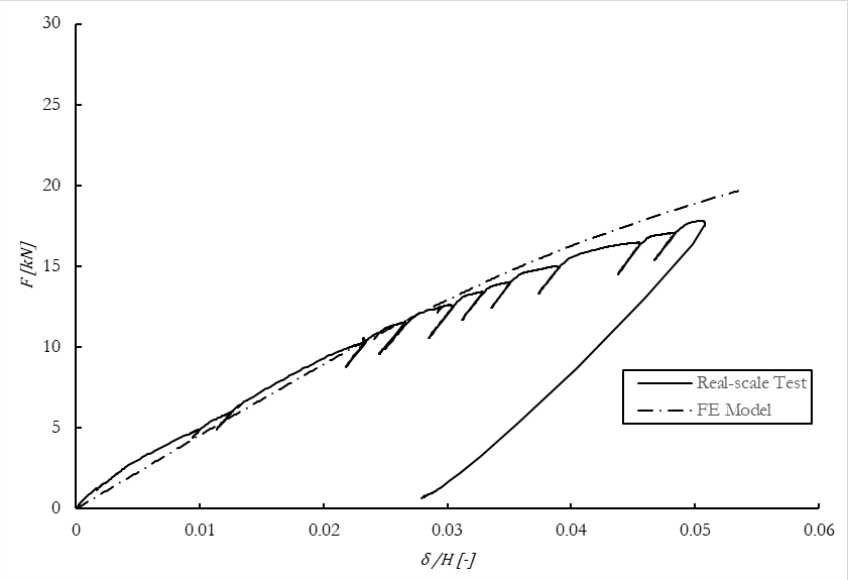

Figure 26 - *Comparison between real-scale test and FE model*

References

Aguirre, C. (2005). Seismic behavior of rack structures. *Journal of Constructional Steel Research*, *61*(5), 607–624. https://doi.org/10.1016/j.jcsr.2004.10.001

Baldassino, N., Bernuzzi, C., di Gioia, A., & Simoncelli, M. (2019). An experimental investigation on solid and perforated steel storage racks uprights. *Journal of Constructional Steel Research*, *155*, 409–425. https://doi.org/10.1016/j.jcsr.2019.01.008

Bernuzzi, C., & Castiglioni, C. A. (2001). Experimental analysis on the cyclic behaviour of beam-to-column joints in steel storage pallet racks. *Thin-Walled Structures*, *39*(10), 841–859. https://doi.org/10.1016/S0263-8231(01)00034-9

Bernuzzi, C., di Gioia, A., Gabbianelli, G., & Simoncelli, M. (2017). Pushover Analyses of Hand-Loaded Steel Storage Shelving Racks. *Journal of Earthquake Engineering*, *21*(8), 1256–1282. https://doi.org/10.1080/13632469.2016.1210063

Bernuzzi, C., Gobetti, A., Gabbianelli, G., & Simoncelli, M. (2014). Warping influence on the resistance of uprights in steel storage pallet racks. *Journal of Constructional Steel Research*, *101*, 224–241. https://doi.org/10.1016/j.jcsr.2014.05.014

Bernuzzi, C., Pieri, A., & Squadrito, V. (2014). Warping influence on the static design of unbraced steel storage pallet racks. *Thin-Walled Structures*, *79*, 71–82. https://doi.org/10.1016/j.tws.2014.01.024

Bernuzzi, C., & Simoncelli, M. (2016). An advanced design procedure for the safe use of steel storage pallet racks in seismic zones. *Thin-Walled Structures*, *109*, 73–87. https://doi.org/10.1016/j.tws.2016.09.010

Bertocci, L., Comparini, D., Lavacchini, G., Orlando, M., Salvatori, L., & Spinelli, P. (2017). Experimental, numerical, and regulatory P-Mx-My domains for cold-formed perforated steel uprights of pallet-racks. *Thin-Walled Structures*, *119*, 151–165. https://doi.org/10.1016/j.tws.2017.06.001

CEN European Committee for Standardization. (2009). *EN 15512, Steel Static Storage Systems - Adjustable Pallet Racking Systems - Principles for Structural Design*.

CEN European Committee for Standardization. (2016). *EN 16681, Steel static storage systems - Adjustable pallet racking systems - Principles for seismic design*.

Comparini, D., Bertocci, L., Salvatori, L., Orlando, M., Lavacchini, G., & Spinelli, P. (2017). Down-Aisle Seismic Behavior of Pallet-Rack Systems : Experimental Tests and Numerical Analyses. *XVII Convegno ANIDIS - L'Ingegneria Sismica in Italia*, 72–81.

Dai, L., Zhao, X., & Rasmussen, K. J. R. (2018). Cyclic performance of steel storage rack beam-to-upright bolted connections. *Journal of Constructional Steel Research*, *148*, 28–48. https://doi.org/10.1016/j.jcsr.2018.04.012

El-Kadi, B., & Kiymaz, G. (2015). Behavior and design of perforated steel storage rack columns under axial compression. *Steel and Composite Structures*, *18*(5), 1259–1277. https://doi.org/10.12989/scs.2015.18.5.1259

Elias, G. C., de Almeida Neiva, L. H., Sarmanho, A. M. C., Alves, V. N., & Barbosa e Castro, A. F. (2018). Ultimate load of steel storage systems uprights. *Engineering Structures*, *170*, 53–62. https://doi.org/10.1016/j.engstruct.2018.05.078

EN1993-1-1. (2005). *Eurocode 3, Design of Steel Structures - Part 1-1: General rules and rules for buildings*.

EN1993-1-3. (2005). *Eurocode 3, Design of Steel Structures - Part 1-3: supplementary rules for cold formed thin gauge members and sheeting*.

EN1998-1-1. (2004). *Eurocode 8, Design of Structures for earthquake resistance - Part 1: General rules, seismic actions and rules for buildings*.

Fajfar, P. (2000). A Nonlinear Analysis Method for Performance-Based Seismic Design. *Earthquake Spectra*, *16*(3), 573–592. https://doi.org/10.1193/1.1586128

Fajfar, P., & Gašperšič, P. (1996). The N2 method for the seismic damage analysis of RC buildings. *Earthquake Engineering and Structural Dynamics*, *25*(1), 31–46. https://doi.org/10.1002/(SICI)1096-9845(199601)25:1<31::AID-EQE534>3.0.CO;2-V

Filiatrault, A., Eeri, M., Higgins, P. S., Wanitkorkul, A., Courtwright, J. A., & Michael, R. (2008). *of Base Isolated Pallet-Type Steel Storage Racks*. *24*(3), 617–639. https://doi.org/10.1193/1.2942375

Foraboschi, P. (2019). Lateral load-carrying capacity of steel columns with fixed-roller end supports. *Journal of Building Engineering*, *26*. https://doi.org/10.1016/j.jobe.2019.100879

Foraboschi, Paolo. (2020). Predictive Formulation for the Ultimate Combinations of Axial Force and Bending Moment Attainable by Steel Members. *International Journal of Steel Structures*, *20*(2), 705–724. https://doi.org/10.1007/s13296-020-00316-6

Gabbianelli, G., Kanyilmaz, A., Bernuzzi, C., & Castiglioni, C. A. (2017). A combined experimental-numerical study on unbraced pallet rack under pushover loads. *Ingegneria Sismica*, *34*(1), 18–38.

Gilbert, B. P., & Rasmussen, K. J. R. (2011). Determination of the base plate stiffness and strength of steel storage racks. *Journal of Constructional Steel Research*, *67*(6), 1031–1041. https://doi.org/10.1016/j.jcsr.2011.01.006

Gusella, F., Lavacchini, G., & Orlando, M. (2018). Monotonic and cyclic tests on beam-column joints of industrial pallet racks. *Journal of Constructional Steel Research*, *140*, 92–107. https://doi.org/10.1016/j.jcsr.2017.10.021

Gusella, F., Orlando, M., & Spinelli, P. (2019). Pinching in Steel Rack Joints: Numerical Modelling and Effects on Structural Response. *International Journal of Steel Structures*, *19*(1), 131–146. https://doi.org/10.1007/s13296-018-0095-x

Hilber, H. M., Hughes, T. J. R., & Taylor, R. L. (1977). Improved numerical dissipation for time integration algorithms in structural dynamic. *Earthquake Engineering & Structural Dynamics Structural Dynamics*, *5*(April 1976), 283–292. https://doi.org/10.1002/eqe.4290050306

Iervolino, I., Galasso, C., & Cosenza, E. (2010). REXEL: Computer aided record selection for code-based seismic structural analysis. *Bulletin of Earthquake Engineering*, *8*(2), 339–362. https://doi.org/10.1007/s10518-009-9146-1

Jovanović, Đ., Žarković, D., Vukobratović, V., & Brujić, Z. (2019). Hysteresis model for beam-to-column connections of steel storage racks. *Thin-Walled Structures*, *142*, 189–204. https://doi.org/10.1016/j.tws.2019.04.056

Kanyilmaz, A., Brambilla, G., Chiarelli, G. P., & Castiglioni, C. A. (2016). Assessment of the seismic behaviour of braced steel storage racking systems by means of full scale push over tests. *Thin-Walled Structures*, *107*, 138–155. https://doi.org/10.1016/j.tws.2016.06.004

Kanyilmaz, A., Castiglioni, C. A., Brambilla, G., & Chiarelli, G. P. (2016). Experimental assessment of the seismic behavior of unbraced steel storage pallet racks. *Thin-Walled Structures*, *108*, 391–405. https://doi.org/10.1016/j.tws.2016.09.001

Kilar, V., Petrovčič, S., Koren, D., & Šilih, S. (2011). Seismic analysis of an asymmetric fixed base and base-isolated high-rack steel structure. *Engineering Structures*, *33*(12), 3471–3482. https://doi.org/10.1016/j.engstruct.2011.07.010

Marra, A. M., Salvatori, L., Spinelli, P., & Bartoli, G. (2017). Incremental dynamic and nonlinear static analyses for seismic assessment of medieval masonry towers. *Journal of Performance of Constructed Facilities*, *31*(4). https://doi.org/10.1061/(ASCE)CF.1943-5509.0001022

Montuori, R., Gabbianelli, G., Nastri, E., & Simoncelli, M. (2019). Rigid plastic analysis for the seismic performance evaluation of steel storage racks. *Steel and Composite Structures*, *32*(1), 1–19. https://doi.org/10.12989/scs.2019.32.1.001

Orlando, M., Lavacchini, G., Ortolani, B., & Spinelli, P. (2017). Experimental capacity of perforated cold-formed steel open sections under compression and bending. *Steel and Composite Structures*, *24*(2), 201–211. https://doi.org/10.12989/scs.2017.24.2.201

Peterman, K. D., Nakata, N., & Schafer, B. W. (2014). Hysteretic characterization of cold-formed steel stud-to-sheathing connections. *Journal of Constructional Steel Research*, *101*, 254–264. https://doi.org/10.1016/j.jcsr.2014.05.019

Petrone, F., Higgins, P. S., Bissonnette, N. P., & Kanvinde, A. M. (2016). The cross-aisle seismic performance of storage rack base connections. *Journal of Constructional Steel Research*, *122*, 520–531. https://doi.org/10.1016/j.jcsr.2016.04.014

Powell, G. H., & Allahabadi, R. (1988). Seismic damage prediction by deterministic methods: Concepts and procedures. *Earthquake Engineering & Structural Dynamics*, *16*(5), 719–734. https://doi.org/10.1002/eqe.4290160507

Rahnama, M., & Krawinkler, H. (1993). *Effects of Soft Soil and Hysteresis Model on Seismic Demands*.

Rossi, B., Jaspart, J.-P., & Rasmussen, K. J. R. (2010). Combined Distortional and Overall Flexural-Torsional Buckling of Cold-Formed Stainless Steel Sections: Experimental Investigations. *Journal of Structural Engineering*, *136*(4), 354–360. https://doi.org/10.1061/(asce)st.1943-541x.0000130

Roure, F., Pastor, M. M., Casafont, M., & Somalo, M. R. (2011). Stub column tests for racking design: Experimental testing, FE analysis and EC3. *Thin-Walled Structures*, *49*(1), 167–184. https://doi.org/10.1016/j.tws.2010.09.002

SAP 2000. (2016). *CSI Analysis Reference Manual for SAP2000* (C. and structures Inc. (ed.)).

Simoncelli, M., Tagliafierro, B., & Montuori, R. (2020). Recent development on the seismic devices for steel storage structures. *Thin-Walled Structures*, *155*(May), 106827. https://doi.org/10.1016/j.tws.2020.106827

Vamvatsikos, D., & Allin Cornell, C. (2002). Incremental dynamic analysis. *Earthquake Engineering and Structural Dynamics*, *31*(3), 491–514. https://doi.org/10.1002/eqe.141

Vamvatsikos, D., & Cornell, C. A. (2004). Applied incremental dynamic analysis. *Earthquake Spectra*, *20*(2), 523–553. https://doi.org/10.1193/1.1737737

Yin, L., Tang, G., Zhang, M., Wang, B., & Feng, B. (2016). Monotonic and cyclic response of speed-lock connections with bolts in storage racks. *Engineering Structures*, *116*, 40–55. https://doi.org/10.1016/j.engstruct.2016.02.032

Zhao, X., Dai, L., & Rasmussen, K. J. R. (2018). Hysteretic behaviour of steel storage rack beam-to-upright boltless connections. *Journal of Constructional Steel Research*, *144*, 81–105. https://doi.org/10.1016/j.jcsr.2018.01.006

Zhao, X., Ren, C., & Qin, R. (2017). An experimental investigation into perforated and non-perforated steel storage rack uprights. *Thin-Walled Structures*, *112*, 159–172. https://doi.org/10.1016/j.tws.2016.11.016

ingegneria sismica
International Journal of Earthquake Engineering
Anno XXXVIII – Num.2 - 2021

ANALISI STATICHE NON LINEARI E DINAMICHE INCREMENTALI PER LA CARATTERIZZAZIONE SISMICA IN DIREZIONE LONGITUDINALE DI SCAFFALATURE PORTAPALLET

Alessandro Mei, Maurizio Orlando, Luca Salvatori, Paolo Spinelli

Dipartimento di Ingegneria Civile e Ambientale, Università degli Studi di Firenze, Italia

ABSTRACT: *In questo lavoro vengono presentati i risultati di una serie di analisi numeriche che confrontano il comportamento sismico di scaffalature metalliche in acciaio formato a freddo usando sia l'analisi statica non lineare (NSA), sia l'analisi dinamica incrementale (IDA). A tale scopo è stato considerato un caso studio al quale sono stati applicati un totale di 140 accelerogrammi naturali progressivamente scalati, oltre a due diverse distribuzioni di forze orizzontali per la NSA, considerando sia le non linerità geometriche (effetti P-Δ), sia utilizzando adeguati elementi finiti per riprodurre il comportamento non lineare dei nodi correnti-montanti ("pinching"). I dati ottenuti dalle IDA sono stati trattati statisticamente e confrontati con quelli delle NSA in termini di vulnerabilità sismica, in particolare in termini di domanda e capacità di spostamento, accelerazione spettrale di collasso e proponendo un indice di danno appropriato in grado di seguire lo stato del sistema all'aumentare dell'accelerazione spettrale. I risultati mostrano che la NSA sottostima la domanda di spostamento del sistema e sovrastima la misura dell'intensità del collasso (accelerazione spettrale di capacità), non risultando quindi a favore di sicurezza.*

KEYWORDS: *Cold-Formed Steel, Nonlinear Static Analysis, Incremental Dynamic Analysis, Seismic Assessment, Damage Index*

Corresponding author: Alessandro Mei, Department of Civil and Environmental Engineering, University of Florence, Italy.
Email: alessandro.mei@unifi.it